JOURNAL OF GEOPHYSICAL RESEARCH, VOL. 97, NO. B11, PAGES 15,099–15,112, OCTOBER 10, 1992

Very Long Period Magnetotellurics at Tucson Observatory: Implications for Mantle Conductivity

GARY D. EGBERT

College of Oceanography, Oregon State University, Corvallis

JOHN R. BOOKER

Geophysics Program AK-50, University of Washington, Seattle

In a companion paper (Egbert et al., this issue) we describe the estimation of very long period ($0.16 < T < 91$ days) magnetotelluric (MT) impedances from 11 years of data collected at the Tucson geomagnetic observatory. Here we discuss the implications of these data for mantle conductivity. Using minimum norm (flattest and smoothest) inversions, we find simple one-dimensional models of electrical conductivity in the depth range 0-1500 km. We use forward modeling, a linearized resolution analysis, and constrained one-dimensional inversions to delineate the range of models which are consistent with the estimated impedances. Although the MT data have limited resolution, large-scale vertical averages of mantle conductivity are well constrained. We reach the following conclusions concerning mantle conductivity beneath Tucson: (1) The upper 200 km has a conductance of order 10^4 Siemens (S). This anomalously high conductance may be concentrated in an aesthenospheric high conductivity layer, but the geometry of the conductive zone is not constrained. (2) Typical conductivities in the transition zone (400-700 km) are ≈ 0.1–0.3 S m^{-1}. A step increase to reach this value at or near the 400 km olivine-spinel phase transition is consistent with, but not required by, the data. An upper mantle which is resistive throughout (0.05 S m^{-1} or less) is not allowed by the data. (3) Resolvable large-scale averages of conductivity increase from ≈ 0.2 S m^{-1} to ≈ 1.0 S m^{-1} between 600 and 900 km depth. A range of models, including those with step increases, and step decreases, at the 670 km seismic discontinuity are consistent with the data. (4) Between 900-1500 km, conductivity increases slowly. Average conductivities in this region are of the order of 1 S m^{-1}, to within a factor of 2 or 3. While limited zones of highly resistive mantle are consistent with the data, a lower mantle which is resistive throughout is not. Models in which conductivity is always above 5 S m^{-1} below 1000 km can also be ruled out. In conjunction with improved laboratory estimates of electrical conductivities of mantle minerals at high temperatures and pressures, these constraints can provide important clues to the composition and physical state of the mantle.

1. INTRODUCTION

Many workers have attempted to resolve the electrical conductivity of the Earth's mantle as a function of depth. However, it has proved frustratingly difficult to advance beyond the general conclusion of *Lahiri and Price* [1939] that the conductivity rises sharply with depth below several hundred kilometers. Indeed, the range of conductivity models which have been proposed suggests uncertainties of nearly 2 orders of magnitude throughout most of the mantle. This is illustrated in Figure 1, where we present a selection of mantle conductivity models from the recent literature. For these models, virtually all of the responses relevant to mantle structure were computed using some variant of the geomagnetic depth sounding (GDS) method. With the GDS approach, the impedances are derived from three-component magnetic field data, together with some information (or simplifying assumptions) about the external source structure (see *Rokityansky* [1982] for a review of different approaches). Unfortunately, the detailed geometry of the sources is never completely known except in rather special cases (e.g., at very long periods, where the morphology of the sources is well approximated as a zonal dipole, so that the impedances can be estimated from the ratio H_z/H_x of vertical to zonal magnetic field components at a single site [*Banks*, 1969; *Schultz and Larsen*, 1983]), and the coherence between magnetic field components is often low. As a result impedances derived from GDS data typically have rather large error bars and are useful over only a limited range of periods. Although some of the variation between models of Figure 1 probably reflects lateral heterogeneity of conductivity (particularly in the uppermost mantle), we believe that the scatter primarily reflects limitations in data quality and variations in processing and interpretation methods.

In this paper we present estimates of mantle conductivity obtained from a combination of very long period magnetotelluric (MT), and GDS data from the geomagnetic observatory at Tucson, Arizona. Analysis of this data is described in detail in a companion paper (*Egbert et al.*, this issue; hereafter referred to as paper 1). Briefly, MT impedances were estimated from 11 years of data, corrected for noninductive near-surface distortion of the electric fields, and combined with equivalent MT impedances obtained from 46 years of GDS data from the Tucson observatory. In contrast to the GDS approach, MT allows direct estimation of impedances which are relatively insensitive to the exact spatial structure of sources [e.g., *Dmitriev and Berdichevsky*, 1979]. For periods $T < 5$ days (where external sources cannot be simply characterized) impedances were estimated from the MT data. For longer periods (where source morphology is typically relatively simple) we used impedances computed from the GDS (i.e., H_z/H_x) transfer functions.

The result is a set of scalar impedance estimates for periods $0.17 < T < 91$ days of unprecedented precision (Figure 1*b*; see also Table 2 and Figure 16 in paper 1). The error bars for the apparent resistivity (ρ) and phase (ϕ) estimates are small compared to the variation of these parameters predicted by the models of Figure 1*a*, which for the most part are grossly inconsistent with the Tucson data. The Tucson MT data are thus capable of distinguishing among the wide range of models given in Figure 1*a* and should allow us to constrain mantle conductivity much more

Paper number 92JB01251.
0148-0227/92/92JB-01251$05.00

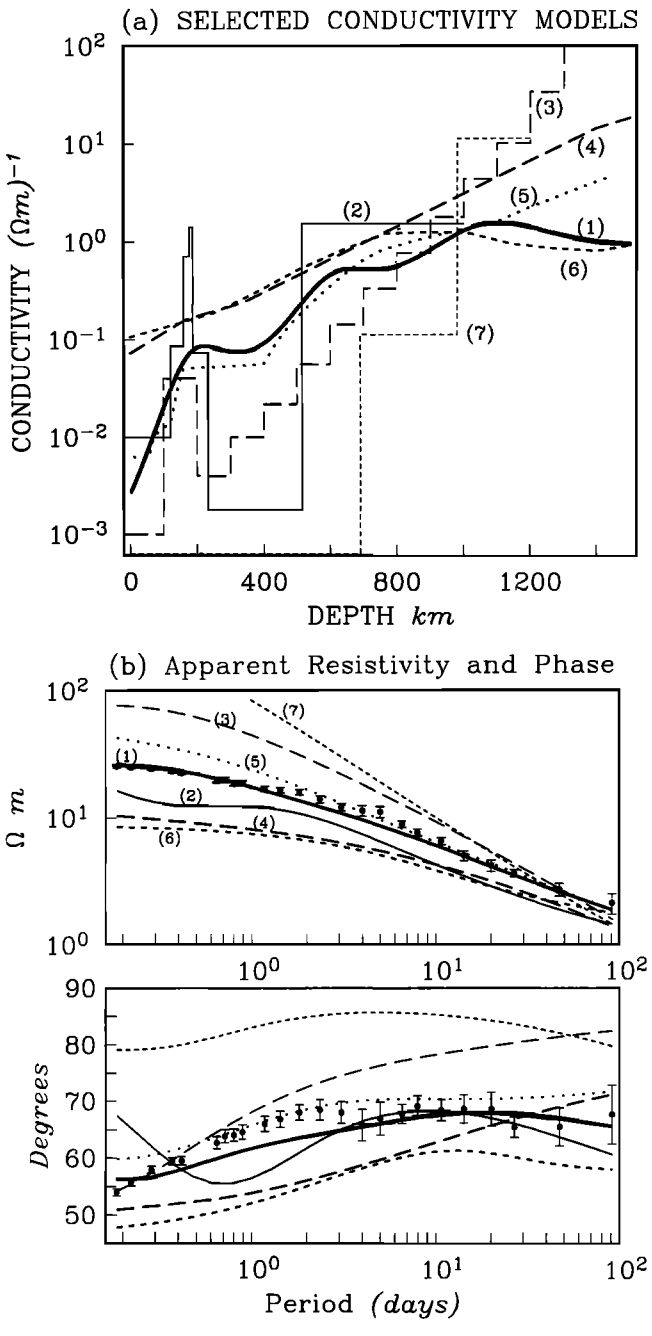

Fig. 1. (*a*) Selected mantle conductivity models. 1, model fit to Tucson data (model 2d from Figure 2); 2, *Larsen* [1977]; 3, *Rokityanski* [1982, p 155]; 4, *Achache et al.* [1981]; 5, *Hobbs* [1983]; 6, *Parker* [1970]; and 7, *Jady and Pattersen* [1983]. The range of model conductivities is 1 to 2 orders of magnitude at all depths. (*b*) Apparent resistivities and phases for the seven models of Figure 1*a*. Most of the models are grossly inconsistent with the Tucson impedances and with each other.

tightly than a casual examination of the existing literature might suggest possible.

As discussed in paper 1, for periods less than one day the ρ and ϕ estimates, while individually consistent, are not mutually consistent with any one-dimensional conductivity model. However, we also showed in paper 1 that conductance profiles corresponding to best fitting models (the so-called "D^+" models of *Parker* [1980]) for a range of data subsets (all data, phase data alone, amplitude data alone) are very similar, giving us some confidence that reliable large-scale vertical averages of mantle conductivity can be inferred from these data. The D^+ models, which consist of infinitesimally thin layers of finite conductance, suggest large scale average conductivities of the order of 0.05 S m^{-1} in the first 200 km, increasing to 0.2–0.3 S m^{-1} between 200 and 700 km depth, and finally to roughly 1.0 S m^{-1} in the lower mantle. In this paper we consider more physically realistic smoothly varying mantle conductivity models, and we attempt to delineate the range of models which are consistent with the Tucson data.

Larsen [1977] has previously presented a model for mantle conductivity based on a preliminary analysis of the Tucson MT data (curve 2 in Figure 1), and he has recently refined his impedance and his mantle conductivity estimates [*Larsen*, 1989; also personal communication, 1987]. The methods of analysis discussed here, and in paper 1, differ markedly from those used by *Larsen* [1975, 1977, 1980, 1989]. In particular, we use overparametrized minimum structure inversions, linearized resolution analysis, and constrained inversions in an effort to identify properties of the Earth's conductivity profile which are required by the data. Our analysis demonstrates that large-scale averages of mantle conductivity are well constrained by these data and that the range of consistent simple conductivity models is in some sense quite small. A number of significant features exhibited by previously reported models, or suggested by laboratory experiments, are clearly not allowed by these data.

2. INVERSION METHODS

To invert the impedances for simple models of mantle conductivity, we used the seminorm minimization approach of *Constable et al.*, 1987] and *Smith and Booker*, 1988]. The basic idea is to find the conductivity model $\sigma(z)$ which minimizes a roughness penalty of the form

$$\|\sigma\|_n = \left[\int \left| \frac{d^n \log \sigma(z)}{d \log z^n} \right|^2 dz\right]^{1/2}, \quad (1)$$

subject to the constraint that the data be adequately fit, i.e., that

$$\sum_{k=1}^{K} \frac{|Z_k[\sigma]-\hat{Z}_k|^2}{s_k^2} < M^2 \quad (2)$$

In (2), $\hat{Z}_k$ is the impedance estimate for the kth period, s_k is the corresponding standard error, $Z_k[\sigma]$ is the impedance predicted at this period by the conductivity profile $\sigma(z)$, and M^2 is the allowable misfit. We consider models fit with $n=1$ (flattest models) and $n=2$ (smoothest models).

Since the full set of estimated impedances considered here cannot be fit to within the statistical estimation errors by any one-dimensional model (paper 1), it is impossible to rigorously justify the exact level of misfit (i.e., M^2 in (2)) which should be considered adequate. We have thus found minimum structure models which achieve a range of misfits above the minimum possible (e.g., Figures 2 and 3). As M^2 approaches the minimum achievable misfit (χ^2_{min}) the models become very similar to the physically unrealistic D^+ models, with conductance concentrated in a series of thin layers. As M^2 is increased, smoother and simpler models result. We consider those features which persist even when the misfit is substantially relaxed to be well constrained by the data. In addition to models fit to the full data set, we also consider models fit to the more nearly self-consistent longer-period subsets (Figure 2). Again, model features which persist when the period range is reduced are more clearly required by the data.

To study the resolving power of the MT data, we use a linearized Backus-Gilbert approach [e.g., *Parker*, 1970]. Because the

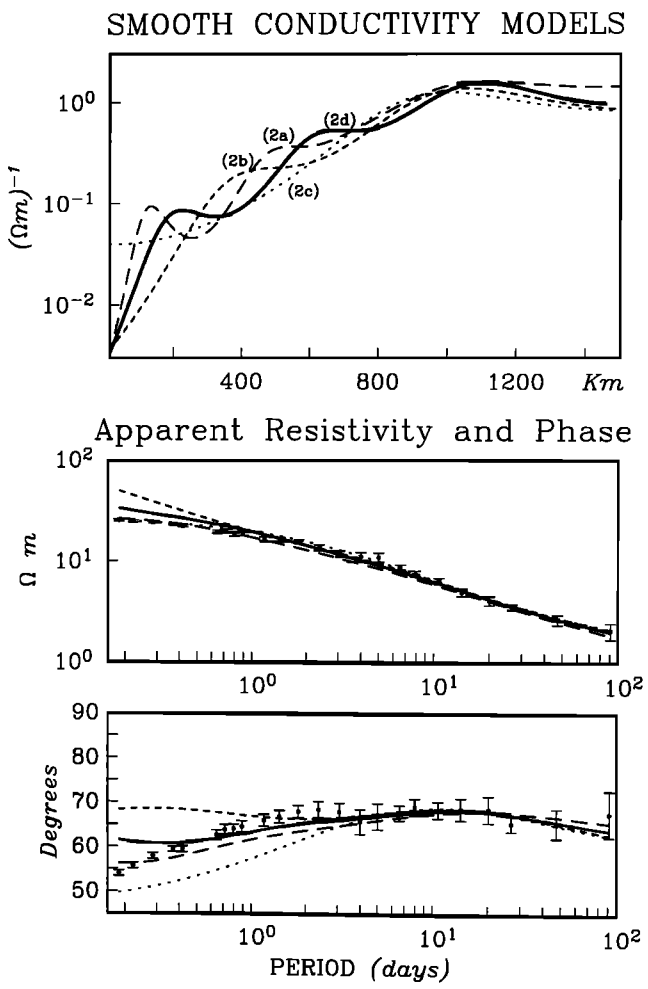

Fig. 2. Flattest models fit to subsets of the data: model 2a, all data, fit to $1.2\times\chi^2_{min}$; model 2b, $T > 1$ day, fit to $1.5\times\chi^2_{min}$; model 2c, $T > 5$ days (geomagnetic depth sounding data only), fit to expected χ^2; model 2d, all data is used but errors for $T < 1$ day are increased by a factor of 5. This model is fit to $1.2\times\chi^2_{min}$, with the misfit normalized by the modified errors.

MT inverse problem is nonlinear, the resolution kernels (Figure 4) only apply rigorously to models linearly close to each other. However, the analysis of *Smith and Booker* [1988] suggests that conductivity models produced by minimum roughness inversions can, to a very good approximation, be interpreted as the true conductivity smoothed through the resolution kernels. In the appendix we expand on this point, and demonstrate its relevance to the Tucson MT data. We show that for models of log conductivity, the resolution kernel $R(z, z_0)$ (i.e., the function corresponding to a horizontal slice at fixed depth z_0 on the vertical axis of Figure 4) can be interpreted as the fractional contribution that conductivity in the true model at a depth z makes to the estimated smooth conductivity at z_0. Resolution kernels for log conductivity models thus provide a good estimate of the averaging length scales inherent in smooth log conductivity models, where conductivity varies by several orders of magnitude. In Figure 4 we shade the central portion of the resolution kernels which accounts for 2/3 of the total conductance at the nominal depth in the smooth model. For purposes of discussion, we consider the width of this zone as the resolution length scale for conductivity estimates at z_0.

To further characterize the range of models which are consistent with the estimated impedances we modified the OCCAM inversion program of *Constable et al.* [1987] to allow conductivities in any set depth range to be constrained in some manner. By seeking constrained models that otherwise minimize the structure penalty subject to a certain level of misfit, we can test hypotheses. This allows us to demonstrate convincingly that certain features of previously published mantle conductivity profiles are not even approximately consistent with the Tucson data.

3. INVERSION RESULTS

Models

To help organize the large number of models to be discussed in this paper, we adopt a standard notation. Models will be referred to by the figures in which they first appear, and the lower case roman letter by which they are labeled in this figure (e.g., model 2a is curve a of Figure 2). All conductivity models for the Tucson data are summarized in Table 1.

Flattest models, which minimize (1) with $n = 1$, are plotted with corresponding predicted ρ and φ responses for three subsets of the data in Figure 2. Note that these models were calculated for

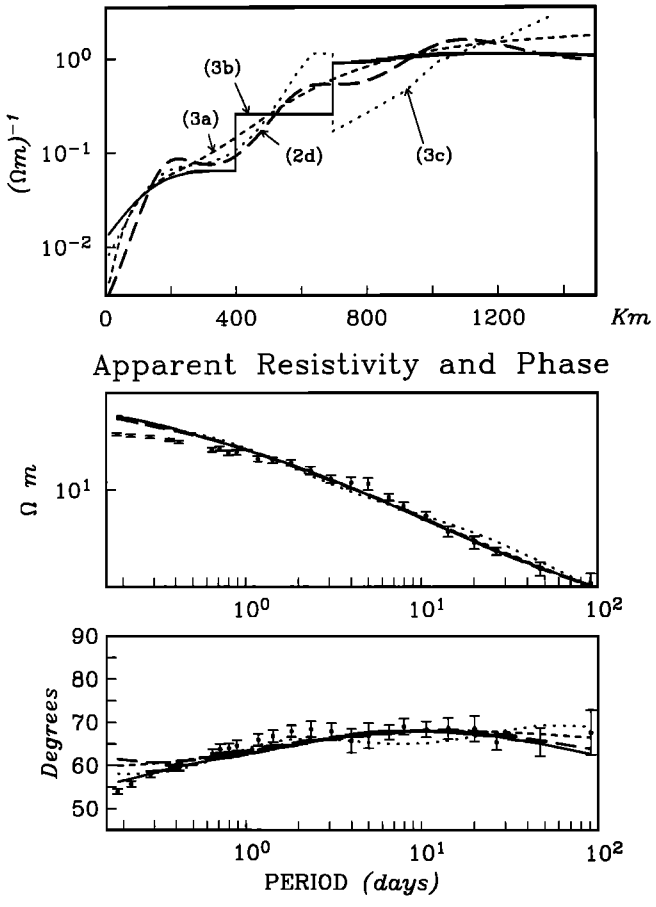

Fig. 3. Three alternative models fit to the combined MT and GDS data. Model 3a minimizes the second derivative norm and is fit to all data with errors for $T < 1$ day increased by a factor of 5. This model, which is fit to $1.5\times\chi^2_{min}$, is very smooth and shows no evidence of steps (compare to model 2d, reproduced from Figure 2, which is fit to within $1.2\times\chi^2_{min}$ of the same data). Model 3b, which has the same misfit as model 3a, has distinct steps at 400 and 670 km depth. The two models yield almost indistinguishable ρ and φ curves except at the longest and shortest periods. In model 3c, conductivity increases to a peak at the bottom of the upper mantle, decreases sharply at the top of the lower mantle, and then increases again. This model does not fit the data quite as well as the other models plotted here, but the fit is at least qualitatively reasonable. The range of models demonstrates the difficulty in resolving small-scale features such as steps or localized gradients in conductivity.

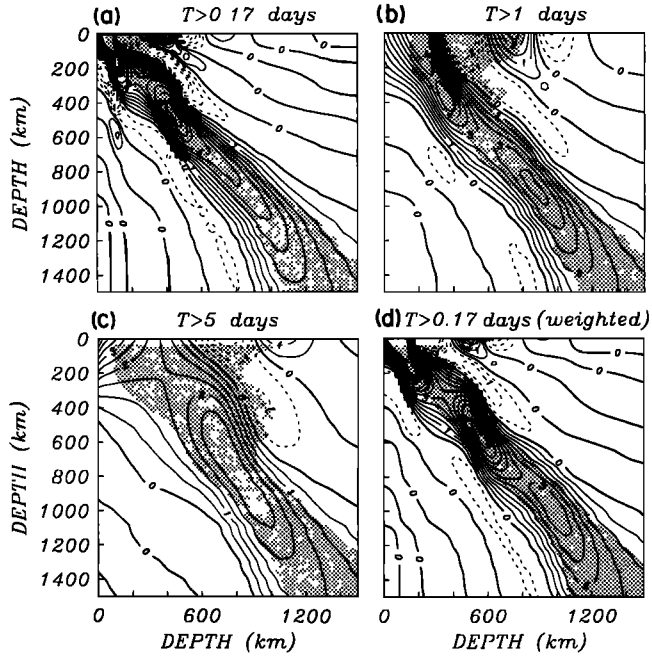

Fig. 4. Resolution kernels $R(z, z_0)$ for the four models of Figure 2. The resolution kernel corresponding to a horizontal slice at a fixed depth z_0 on the vertical axis gives the relative fractional contribution that conductivity in the true model at depth z makes to the estimated smooth conductivity model at z_0. Shaded region represents the central portion of the resolution kernels that accounts for 2/3 of the total conductance at the nominal depth (z_0) in the smooth model.

a flat, infinitely deep Earth. However, *Weidelt* [1972] shows how to simply transform flat Earth models to a spherically symmetric Earth. The models plotted (and all others discussed in this paper) have been transformed to spherical Earth profiles. Model 2a is fit to the full data set ($0.17 \le T \le 91$ days), with a target squared misfit level 20% larger than the minimum achieved by the best fitting D^+ model ($M^2 = 1.2\,\chi^2_{\min}$). For model 2b, impedances restricted to periods $T \ge 1$ day are fit to $M^2 = 1.5\,\chi^2_{\min}$, and for model 2c, the nine complex GDS impedances ($5 \le T \le 91$ days) are fit to the expected misfit (M^2 = number of degrees of freedom = 18). These three models are very similar below about 600 km depth and all fit the long period GDS data well. The responses of the three models diverge significantly at short periods, and only model 2a is even approximately consistent with the MT impedances for $T < 1$ day. However, for $1 < T \le 5$ days the fit of model 2b is significantly better than the fit of 2a. It is not clear whether the mid-upper mantle structure of model 2b (which fits the self-consistent long-period data better) or model 2a (which fits all of the data at least approximately) should be preferred. Model 2d represents a compromise (between 2a and 2b) which fits the self-consistent long period data about as well as 2b without completely ignoring the short-period MT data. To find this model, we increased the errors for the data in the range $T < 1$ day by a factor of 5 and then fit the modified data to $1.2\,\chi^2_{\min}$. This is our preferred model, although all of the models are similar below 200 km (conductivities within a factor of 2 or less and depths to structural features within 100 km or less). This reinforces the conclusion reached in paper 1: the large-scale averages of deep mantle conductivity are relatively insensitive to the manner in which the inconsistency in the shortest-period data is resolved.

All of the models of Figure 2 share some general features which seem to be required. Conductivity increases with depth by several orders of magnitude with $\sigma \approx 0.2$ S m^{-1} by around 400 km and $\sigma \approx 1.0$ S m^{-1} by around 1000 km. Below this depth conductivity levels off. These conductivities are consistent with the D^+ conductance profiles discussed earlier and in paper 1.

The three smooth models fit to subsets of the MT data (models 2a, 2b, and 2d) are also similar at smaller scales, with two zones of relatively rapid conductivity increase (near 400 and 800 km). However, these details in the conductivity profile can be eliminated or altered without increasing the misfit an implausible amount. Figure 3 illustrates this point nicely. Model 3a, the smoothest model ($n = 2$ in (1)) which fits the data to within $1.5\,\chi^2_{\min}$, has conductivities which are similar to the models of Figure 2, but between 100 and 1000 km this conductivity profile is essentially featureless. Model 3b, which has discontinuous increases in conductivity at 400 and 700 km, also fits the full data set within $1.5\,\chi^2_{\min}$. The two models predict apparent resistivities and phases which are virtually indistinguishable except at the longest and shortest periods. Thus, although the MT data are consistent with (and even suggest) step discontinuities (or at least sharp localized gradients) of conductivity near the 400 and 670 km seismic discontinuities, it is impossible to argue that any such structures are required by these data. In fact, much greater variations in conductivity are allowed. Model 3c actually reverses the sign of the step in the conductivity profile at 700 km and is still reasonably consistent with the data. Relative to the systematic biases and inconsistencies in the Tucson impedances at short periods, the differences between the predicted responses for all four models of Figure 3 are unimpressive, indicating that a substantial increase in data quality would be required to resolve localized gradients in conductivity. Considering the uncertainties that may be introduced into geomagnetic data from source complications and lateral heterogeneity of conductivity (see paper 1), it seems unlikely that induction data by itself will ever be able to distinguish between models 3a and 3b.

The short-period ($T < 1$ day) MT impedances suggest the presence of a high conductivity layer in the uppermost mantle.

TABLE 1. Summary of Tucson Conductivity Models Discussed in Text

Model	Data Set	RMS D^+	RMS Model	Constraints
2a	1	3.43	3.76	
2b	2	1.21	1.48	
2c	3	0.60	1.00	
2d	4	1.32	1.44	
3a	4	1.32	1.62	
3b	4	1.32	1.62	
3c	4	1.32	1.84	
5a	2	1.21	3.4	σ=100 S, z>1000
5b	2	1.21	2.5	σ=5 S, z>1000
5c	2	1.21	4.8	σ=0.001 S, 700<z<1900
5d	2	1.21	3.3	σ=0.5 S, 700<z<1900
6a	2	1.21	4.3	σ=0.05 S, 0<z<700
6b	2	1.21	2.9	σ=0.05 S, 200<z<700
6c	2	1.21	5.9	σ=1.0 S, 400<z<700
6d	2	1.21	2.8	σ=1.0 S, 500<z<700
7a	1	3.43	8.9	σ=0.01 S, 0<z<200
7b	1	3.43	16.0	σ=0.01 S, 0<z<200; σ=0.1 S, 200<z<400

Models are denoted by the figure in which they first occur, together with the lowercase roman letter which identifies them in that figure. Data sets used are 1, $.17 < T < 91$ days (all data); 2, $1 < T < 91$ days; 3, $5 < T < 91$ days (GDS data only); and 4, $0.17 < T < 91$ days, with errors multiplied by 5 for $T < 1$ day. D^+ RMS gives the RMS misfit achieved by the best fitting (D^+) model for the data set used. RMS model gives the RMS misfit actually achieved by the model. For constrained models the depth range given in the last column (in kilometers) was constrained to the specified conductivity. For these models, model misfits are essentially the minimum possible subject to the constraints.

Models which fit the short-period MT data have such a layer between 100 and 300 km (e.g., 2a and 2d) As the misfit is relaxed the layer broadens and ultimately merges with the higher conductivity region near 400 km, but it does not disappear. In all cases the total conductance of this layer is $\approx 10^4$ S. It is noteworthy that, while ρ and ϕ are not jointly consistent at the shortest periods, D^+ models fit to both data subsets also have a conductance of $\approx 10^4$ S in the upper 200 km (paper 1).

Resolution

Resolution kernels for the four models of Figure 2 are plotted in Figure 4. Resolution length scales range from 200 to 500 km or more, with the best resolution (<300 km) between 300 and 1000 km for the inversions using all data. Over this depth range the averaging kernels are centered on the nominal depth. Below 1000 km the kernels are significantly wider and are centered above the sampling depth. For all four models, resolution is very poor in the upper 200 km, where the kernels are broad and have large negative sidelobes.

The conductivity estimates at nominal depths of 900 and 1300 km are very nearly identical but represent averages over nearly disjoint depth ranges, 800-1100 km and 1100-1500 km. Thus, while averaging length scales in the lower mantle are large (≈300–500 km for all models), the resolution kernels imply that the flattening of the conductivity profile at depths greater than 1000 km is in some sense required by the data. We stress that these conclusions apply only to the large-scale averages of log conductivity. Model 3c provides an example of an acceptable, physically plausible conductivity profile with much steeper gradients in the lower mantle. This model has high conductivities at the bottom of the transition zone, a discontinuous decrease in conductivity (approximately one order of magnitude) as the upper mantle is entered, and then relatively steep gradients in the upper part of the lower mantle. As demonstrated in the appendix, averages of this model computed using the broad resolution kernels for the smooth model at depths of 900 and 1300 km are both of order 1, as implied by the resolution analysis. However, to allow such steep gradients in the lower mantle, the low-conductivity zone near 700 km must be accompanied by a sharp increase in conductivity just above the transition zone.

Resolution kernels for the long period ($T \geq 5$ days) Tucson GDS data, are very broad (≈500–600 km) and have significant negative sidebands everywhere in the upper mantle (Figure 4*c*). By using the full MT data set, resolution between 200 and 700 km is much improved (Figures 4*a* and 4*d*), even with the large error bars which must be assumed to accommodate the systematic failure of the one-dimensional model at the shortest periods. In fact, including only the longer period ($1 < T \leq 5$ day) MT data (Figure 4*b*) results in a dramatic improvement in resolution for depths of 400-700 km. Clearly, impedances in the period range $1 < T \leq 5$ days, are critical for constraining upper mantle conductivity. To a great extent, the large range of upper mantle conductivities exhibited by the models of Figure 1 reflects the poor resolution of the long-period ($T > 5$ days) GDS data upon which most of these models are based.

Hypothesis Testing

In several of the models in Figure 1, mantle conductivity continues to rise steeply below 1000 km to values of 10-50 S m^{-1} by depths of 1500 km. Such models fit our impedance estimates very poorly (Figure 1*b*). In particular, models 3 [*Rokityansky*, 1982] and 7 [*Jady and Pattersen*, 1983] have phases that are much too high at long periods (indicating that the model conductivity gradient is too steep at depth). Model 4 [*Achache et al.*, 1981] does not increase as steeply in the lower mantle but is more conductive at shallow depths; thus it still has conductivities exceeding 10 S m^{-1} above 1500 km. The phase response for this model is more reasonable at the longest periods, but due to the relatively high values of model conductivity in the upper mantle, the apparent resistivity is much too low at all periods.

To demonstrate more rigorously that such high conductivities are not allowed above 1500 km depth, we constrained the conductivity below 1000 km to match model 3 of Figure 1 *Rokityansky*, 1982] and found the layered one-dimensional model that best fits the self-consistent longer-period ($T > 1$ day) data subject to this constraint. The resulting model and predicted apparent resistivities and phases are given in Figure 5. The minimum normalized root mean square (RMS) misfit with the lower mantle constrained to be so conductive is 3.4 (compared to a minimum RMS of 1.2 for unconstrained one-dimensional models and an RMS of 1.5 for the smooth reference model in Figure 5). Note that the fit to the apparent resistivities is quite good except at the longest period but that the phases required by a highly conducting deep mantle are systematically too high for $T > 10$ days. It is worth noting that the model of *Rokityansky* [1982] is based primarily on apparent resistivity data, which he considers more reliable than phase data. Although with perfect and complete data, apparent resistivity and phase are completely redundant [e.g., *Weidelt*, 1972], for data with finite bandwidth, the phase clearly contains useful additional information which should not be ignored. In fact, the phase data actually provide a tighter upper bound on deep conductivity averages (at least in this case). Figure 5*b* gives the best fitting model with conductivity below 1000 km depth constrained to be 5 S m^{-1}. The deviation of the phase at the longest periods is nearly as severe as for the more conductive lower mantle model of Figure 5*a*. We conclude that the average conductivity in the lower mantle (between 1000 and 1500 km depth at least) is less than 5 S m^{-1}.

Constrained inversions also show that a very resistive lower mantle is not allowed by the Tucson data. The minimum RMS achievable with conductivity constrained to be 10^{-3} S m^{-1} between 700 and 1900 km, as suggested by laboratory measurements of perovskite and magnesiowustite conductivities at lower mantle conditions [*Li and Jeanloz*, 1987, 1990*a*], is 4.8 (Figure 5*c*). The resistive zone has a substantial effect on both ρ and ϕ curves, particularly for $10 < T < 50$ days, where ρ becomes nearly flat and ϕ is substantially reduced. When the constraint is relaxed substantially, to 0.5 S m^{-1}, the result is very similar (Figure 5*d*). We conclude that, while limited regions of the lower mantle may be highly resistive (the best fitting D^+ models are perfectly resistive almost everywhere), the entire lower mantle cannot be. Average conductivities between 700 and 1500 km must be 1 S m^{-1}, within a factor of 2 or 3.

The smooth model derived from the Tucson GDS data (model 2c), and some other models derived only from long-period GDS data (e.g., model 7, Figure 1; see also *Roberts* [1986] and *Schultz and Larsen* [1990]), suggest that the entire upper mantle may be relatively resistive, with the initial zone of high conductivity at depths of 600-700 km or more. However, adding the MT data rules out a relatively resistive mid mantle. In Figures 6*a* and 6*b* we present the results of one-dimensional inversions in which the upper mantle is constrained to be moderately resistive. The minimum achievable RMS with an upper mantle conductivity of 0.05 S m^{-1} is 4.3 (Figure 6*a*). Again, the discrepancy is most

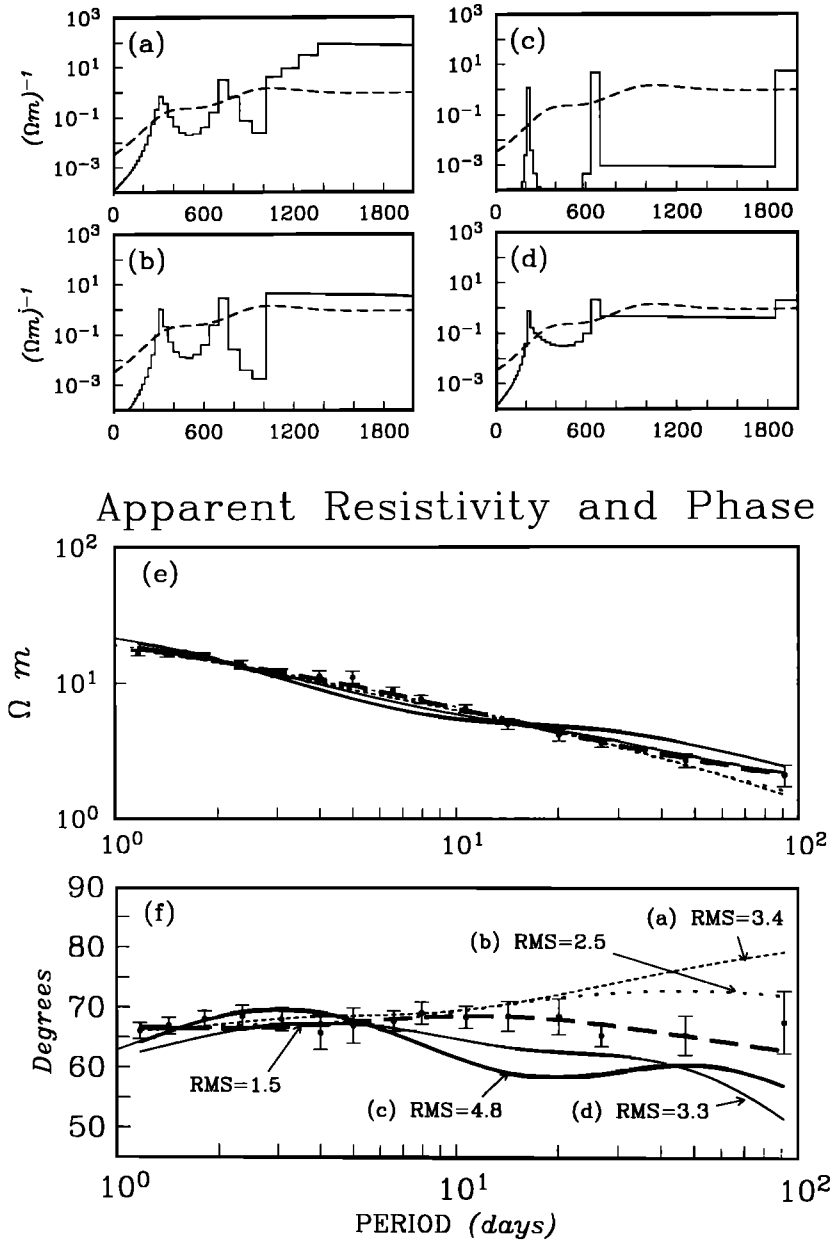

Fig. 5. (*a-d*) Models and computed responses obtained from inversion of impedances for $T > 1$ day, with constraints on lower mantle conductivities. Because we sought to minimize the misfit, the constrained layered models are very rough, with most of the conductance concentrated in a small number of layers. Note that after transformation of the models to a spherical Earth profile the conductivity is no longer exactly constant in each layer. (*e* and *f*) Predicted ρ and φ curves; the RMS misfit achieved is given in Figure 5*f*. For comparison the smooth model fit to the same data set with no constraints (model 2b) and the corresponding ρ and φ are plotted as the heavy dashed lines. Model a is the best fitting model with the deep mantle (below 1000 km) constrained to be very conductive, in agreement with the model of *Rokityanski* [1982] (model 3 of Figure 1). Model b is constrained to be moderately conductive (5 S m^{-1}) below 1000 km. Both of these models predict phases which are significantly too high at the longest periods. Model c is the best fitting model with the lower mantle (700-1900 km depth) constrained to be very resistive (0.001 S m^{-1}). Model d is constrained to be 0.5 S m^{-1} between 700 and 1900 km. Models c and d yield phases that are systematically too low (by ≈ 10°) for $T > 10$ days.

obvious in the phase curve at periods $1 < T < 3$ days. When the upper 200 km are not constrained, the overall fit is improved (RMS = 2.9, Figure 6*b*), but the phase discrepancy persists. Decreasing the constrained conductivity further (e.g., to 0.01 S m^{-1}) leads to similar but even larger systematic misfits.

Models in which the high conductivity of the lower mantle extends up to 400 km depth can also be ruled out. Figure 6c gives the best fitting model with conductivities between 400 and 700 km depth constrained to the 1 S m^{-1} value typical of the lower mantle. With this constraint, ρ is much too low over the entire period range. Moving the top of the high-conductivity zone down to 500 km depth improves the fit noticeably, but ρ is still systematically too small. We conclude that average conductivities in the transition zone (400-700 km) are well below 1 S m^{-1} but not substantially less than 0.1 S m^{-1}.

As a final test we constrained the upper 200 km to be relatively resistive (0.01 S m^{-1}; total layer conductance 2×10^3) and fit the full impedance data set. With this constraint, the minimum

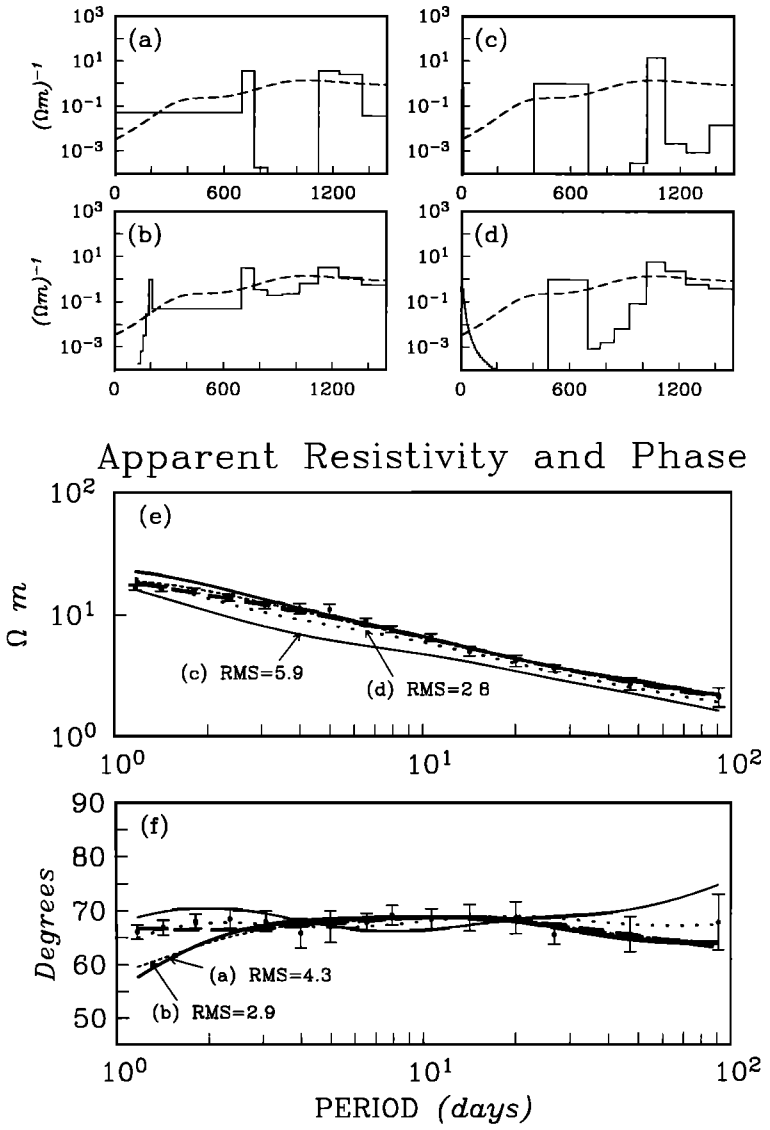

Fig. 6. (*a-d*) Models and (*e-f*) computed responses obtained from inversion with constraints on upper mantle conductivity. As in Figure 5 the heavy dashed lines give the unconstrained smooth model and responses. Model a is the best fitting model with upper mantle constrained to be moderately resistive (0.05 S m^{-1}) between 0 and 700 km. (*b*) As for model a, but with no constraint on the upper 200 km. Both models a and b fit the Tucson data for $T > 3$ days but not the relatively high phases for $1 \leq T \leq 3$ days. Model c is the best fitting model with conductivity between 400 and 700 km constrained to 1 S m^{-1} (i.e., the average conductivity inferred for the lower mantle). This model does not fit the apparent resistivities at any periods beyond 1 day. In model d restricting the conductive zone to depths below 500 km improves the fit dramatically, but apparent resistivities are still systematically too low. This demonstrates that the average conductivity in the transition zone (400-700 km) is significantly lower than the 1 S m^{-1} value typical of the lower mantle.

achievable RMS increases from 3.6 to 8.9 (Figure 7*a*). Forcing the upper mantle to be this resistive makes the predicted phases roughly 10–15° too high and elevates apparent resistivities at the shortest periods. (See also model 2b, which fits only the long-period data and is relatively resistive above 200 km.) Fitting the short-period ($T < 1$ day) data even approximately apparently requires this shallow, 10^4 S conductor. In fact, even the best fitting constrained model has a thin layer of approximately this conductance just below 200 km depth. If the conductivity between 200 and 400 km is also constrained (to 0.1 S m^{-1}) to eliminate this layer, the inconsistency becomes much greater (RMS = 16.0; Figure 7*b*). We conclude that the upper 200 km has a total conductance of the order of 10^4 S. As indicated by the resolution kernels, and the range of acceptable models considered above, no geometrical details of this conductive zone within the uppermost mantle are constrained.

Uncertainties

Our estimates of deep (> 1000 km) conductivity are largely determined by the GDS data, and several assumptions are required to justify the conversion of the GDS transfer functions to equivalent MT impedances. The assumption that the external sources are well approximated as a geomagnetic axial dipole is probably reasonable at a mid-latitude observatory such as Tucson for $5 \leq T \leq 100$ days [*Banks*, 1969; *Schultz and Larsen*, 1983, 1987]. The assumption that the Earth response is completely one-dimensional, even at these long periods, is perhaps not so reasonable [e.g., *Roberts*, 1986; *Schultz and Larsen*, 1990]. In partic-

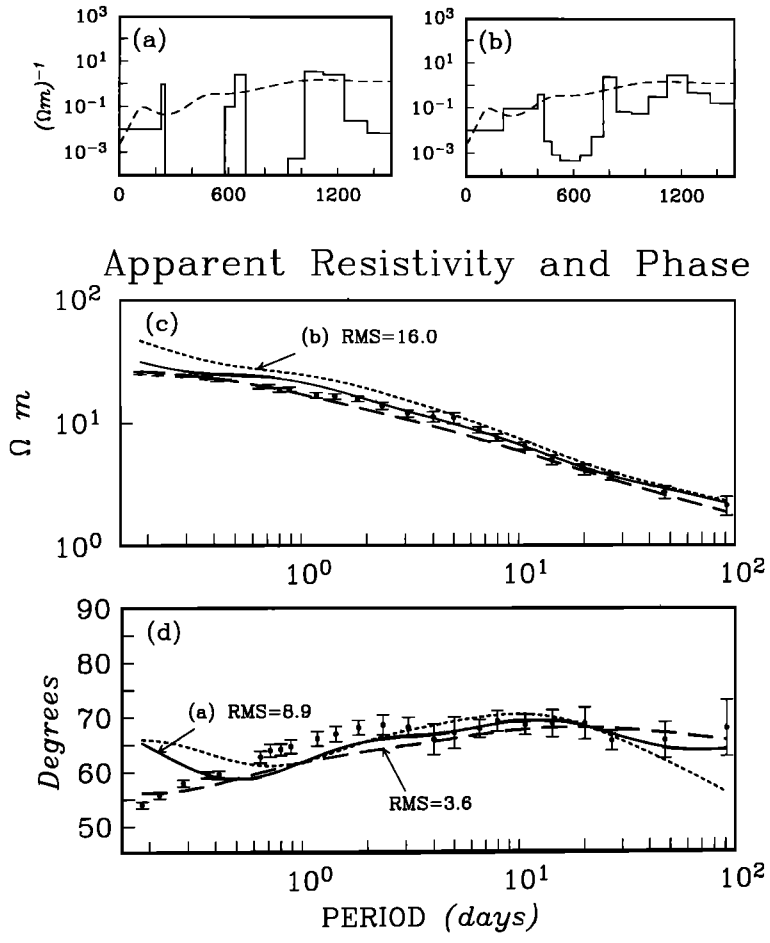

Fig. 7. (*a* and *b*) Models and (*c* and *d*) computed responses with upper 200 km constrained to be resistive (0.01 S m^{-1}). The phase at short periods ($T < 0.5$ days) is too high, and a high-conductivity layer occurs just below 200 km. (*b*) When conductivities between 200 and 400 km are constrained (to 0.1 S m^{-1}) to eliminate this layer (model b), the fit is substantially worse. A conductance of $\approx 10^4$ *S* is required in the upper 200 km to match the short-period phase and apparent resistivity even approximately.

ular, it is not clear how large-scale heterogeneities which may be present in the upper mantle beneath the southwestern United States [*Schmucker*, 1970; *Porath and Gough*, 1971], will affect very long-period GDS transfer functions. This represents an important uncertainty which deserves further attention.

Inferences about the nature of the shallow conductive layer are complicated by the possibility of multidimensional contamination of the shortest-period MT data. Two-dimensional modeling of the coast and Gulf of California show that the depression of the MT phase (relative to that predicted for a model without the shallow high conductivity layer) could be explained by electric currents induced in the ocean, if the lower crustal resistance (thickness times resistivity) is high enough ($2–3 \times 10^9$ ohm m^2) to keep these currents trapped near the surface. As discussed in detail in paper 1, we consider this unlikely. Although there are probably lateral variations of conductivity in the upper mantle in this region, we believe that any geologically reasonable multidimensional model that can explain these data will will include a large-scale high-conductance region (10^4 S or so) in the upper 200 km of the mantle.

4. DISCUSSION

The models of Figure 1 have a range of 1 to 2 orders of magnitude at all depths. This suggests a much greater degree of uncertainty in mantle conductivity than the Tucson MT data allow. Since different models emphasize data from different geographic regions, some of the variability may be the result of lateral heterogeneity. This is almost certainly important in the uppermost mantle. However, studies of lateral variations deeper in the mantle [*Roberts*, 1986; *Schultz and Larsen*, 1990] do not report anything like the order of magnitude variations exhibited by the models in Figure 1. We conclude that the large range of models is due to variations in data quality, processing techniques, and inversion methods, not lateral variation.

The large-scale averages of electrical conductivity are sufficiently tightly constrained by the Tucson data that they should be an important constraint on mantle composition and conditions. For instance, the substantial effect of iron content on olivine conductivity is now well established [e.g., *Mao and Bell*, 1977; *Schock et al.*, 1989], and both theory and experiment suggest that similar results should hold for lower mantle phases [*Li and Jeanloz*, 1990*b*, 1991*b*]. It is thus reasonable to suppose that conductivity will provide a useful constraint on the iron content of the lower mantle. Unfortunately, recent controversy regarding laboratory measurements relevant to deep mantle conductivity [*Peyronneau and Poirier*, 1989; *Li and Jeanloz*, 1991*b*; *Wood and Nell*, 1991] make exploitation of such a constraint difficult at present.

The diamond anvil measurements of *Li and Jeanloz* [1987, 1990*a*] for perovskite (Pv) and for mixtures of Pv and magnesiowustite (Mw) (both 12 at. % iron) at pressures up to 80 GPa and temperatures up to 3500°K suggest that these silicates would be very resistive ($< 10^{-3}$ S m^{-1}) at lower mantle conditions. While locally highly resistive regions in the mantle (balanced by nearby highly conductive regions) can never be ruled out by any conceivable geomagnetic data, the Tucson results imply a well-determined integrated conductivity (conductance) of the order of 10^6 S between 700 and 1500 km. A maximum conductance of only 10^3 S for a Pv+Mw lower mantle, as implied by the low conductivities reported by Li and Jeanloz, is clearly ruled out.

In more recent experiments the same authors have shown that conductivity of lower mantle phases may be strongly affected by both water and iron content. Adding ≈4 wt % water to pyroxene before high-pressure synthesis resulted in an assemblage of two phases (perovskite + a hydrous silicate phase) which was 3 orders of magnitude more conductive than perovskite alone at lower mantle conditions [*Li and Jeanloz*, 1991*a*]. However, such a large volume of water in the lower mantle seems unlikely. Increasing iron content from 10 at. % to 20 at. % increases the conductivity of Pv+Mw assemblages up to 6 orders of magnitude [*Li and Jeanloz*, 1990*b*, 1991*b*]. This yields conductivity estimates at ≈1200 km depth of ≈20 S m^{-1} (Figure 8). Assuming that the lower mantle is anhydrous, these results, together with the Tucson data, suggest an iron content just below 20 at. %. This would imply that the lower mantle is enriched in iron relative to the upper mantle (as suggested on the basis of other geophysical evidence [e.g., *Anderson*, 1989]).

However, other experimental estimates of silicate conductivities at lower mantle conditions appear to contradict the results of Li and Jeanloz. *Peyronneau and Poirier* [1989] measured conductivities of similar mineral assemblages in a diamond anvil cell at pressures of ≈40 GPa and temperatures from 25°C to ≈400°C. Their data are fit well by a single conductivity mechanism with an activation energy of 0.35 eV, and they report essentially identical conductivities for pure Pv and Pv+Mw assemblages. Extrapolation of their results for an iron content of 11 at. % to lower mantle temperatures yields conductivities of roughly 1 S m^{-1} at 1000 km depth. This value is in good agreement with the induction data but is probably a lower bound because additional mechanisms for charge transport with higher activation energies may become important at higher temperatures. *Peyronneau and Poirier* [1989] also show large increases in conductivity with increasing iron content. Their estimates of conductivity for a mantle with 16 at. % iron are a factor of 30 too high at 1000 km (Figure 8), and thus argue against an iron rich lower mantle.

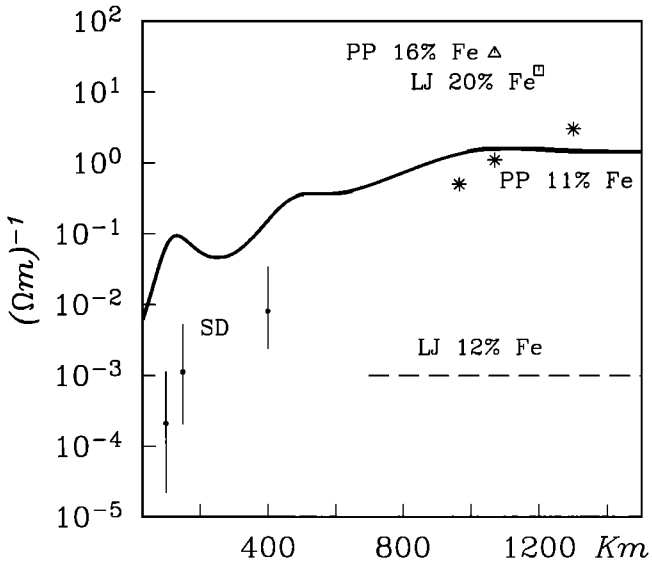

Fig. 8. Smooth conductivity model (model 2d), plotted with laboratory estimates of conductivity for comparison. The solid dots with error bars (SD) are estimates of olivine conductivity obtained by combining mantle temperatures given by *Verhoogen* [1980] with the empirical conductivity-temperature relationship of *Shankland and Duba* [1990]. The asterisks (PP) give estimates of conductivity of perovskite and perovskite-magnesiowustite assemblages containing 11 at. % iron, derived from the results of *Peyronneau and Poirier* [1989]. The triangle gives the corresponding result for 16 at. % iron at a depth of 1070 km. The dashed line (LJ) is the upper bound on perovskite and perovskite-magnesiowustite conductivity given by *Li and Jeanloz* [1990*a*] for 12 at. % iron content, and the square gives the estimated conductivity at 1200 km for an iron rich (20 at. %) perovskite-magnesiowustite assemblage. See discussion in text.

The activation energies estimated by both groups (0.35 by Peyronneau and Poirier and 0.20 by *Li and Jeanloz* [1991*b*]) imply only small (10-20%) temperature-related increases in conductivity between 700 and 1500 km for reasonable lower mantle geotherms [e.g., *Verhoogen*, 1980]. This is in good agreement with the flat conductivity profiles suggested by our results. However, it is likely that the effect of pressure on conductivity is greater than temperature. *Li and Jeanloz* [1991*b*] estimate a pressure dependence for iron rich Pv+Mw of the form $d \log \sigma/dP \approx 0.02$ GPa^{-1}. This would imply conductivity increases by factors of approximately 3 and 6 at depths of between 1000 and 1500 and between 700 and 1500 km, respectively. The results of Peyronneau and Poirier suggest an even steeper deep conductivity gradient due to pressure. Extrapolating their conductivity-temperature relation for perovskite samples (11 at. % iron) synthesized at 37, 42, and 52 GPa yields the conductivity estimates at roughly 965, 1070, and 1300 km depth shown as asterisks in Figure 8. Such high gradients could be accommodated by the Tucson data if conductivity is high at the base of the upper mantle and decreases sharply at the top of the lower mantle (e.g., model 3c). In light of the orders of magnitude discrepancy between results from different laboratories, however, we see no reason to take such a detailed model seriously at present.

In addition to iron content, conductivity of lower mantle minerals may also be strongly affected by oxygen fugacity [*Wood and Nell*, 1991; *Sherman*, 1991]. Indeed, it is quite possible that the very large differences in laboratory estimates of conductivity reflect differences in the oxidation state of the samples tested. *Sherman* [1991] also points out that because of this sensitivity to oxygen fugacity, electrical conductivity profiles may ultimately be able to help constrain the oxidation state of the lower mantle.

Relative to the limited and contradictory laboratory results for perovskite and magnesiowustite in the lower mantle, the electrical conductivity of dry olivine at upper mantle pressures and temperatures is reasonably well understood. A large number of experimental results are reviewed by *Shankland and Duba* [1990], who summarize the data with

$$\sigma = 46.9 \exp(-1.28/kT) + 5.22\times10^8 \exp(-3.90/kT) \quad (3)$$

Using estimates of upper mantle temperatures [*Verhoogen*, 1980] in this relation suggests a shallow upper mantle 1 to 2 orders of magnitude more resistive than the Tucson model (Figure 8). This discrepancy is not unique to our results. Anomalously conductive layers in the upper few hundred kilometers of the mantle have been inferred from a number of previous MT studies (e.g., models 2 and 3 in Figure 1). These high conductivity layers (HCLs) have

typically been interpreted as evidence for partial melting in the aesthenosphere [*Oldenburg*, 1981; *Waff*, 1974; *Shankland et al.*, 1981]. However, the simple existence of a melt fraction is insufficient to cause high conductivity. It must be interconnected over large distances. *Waff* [1980] has pointed out the thermodynamic difficulties associated with this interconnection, and major uncertainties remain, because relevant experiments are limited. Other possibilities, such as small amounts of water [*Tozer*, 1981], carbon [*Duba and Shankland*, 1982], or hydrogen [*Karato*, 1990] have been suggested, but these rest on even slimmer experimental evidence.

The conductance of the shallow HCL inferred from the Tucson data is about 10^4 S. Its conductance and depth are very similar to the HCLs reported beneath young oceanic lithosphere [*Filloux*, 1977, 1980; *Oldenburg*, 1981; *Wannamaker et al.*, 1989; *Ferguson et al.*, 1990]. HCLs also occur under continental lithosphere but typically have an order of magnitude less conductance (see *Rokityansky* [1982, chapter 5] for a review). A notable exception is the apparent 10^4 S HCL under the Fennoscandian Shield [*Jones*, 1982]. However, *Osipova et al.* [1989] interpret this high conductance to be an artifact of source field contamination by the auroral electrojet. Thus the shallow upper mantle under Tucson is clearly anomalously conductive, which provides support for *Goughs* [1984] contention that the southwestern United States overlies a region of upwelling upper mantle (see also *Wilson* [1990]).

As discussed earlier, a relatively resistive zone underlying an upper mantle HCL is allowed by the Tucson data. The low conductivity predicted by (3) between 200 and 400 km can therefore be reconciled with our model. However, near 400 km, extrapolation of (3) yields conductivities which are much too small to be consistent with the induction data. Equation (3) does not include pressure dependence. However, the effects of pressure on the two conduction mechanisms inferred for olivine (hopping of electron holes and ionic conduction) most probably oppose each other [*Shock et al.*, 1989; *Shankland and Duba*, 1990]. Furthermore, ionic conduction, which should be inhibited by increasing pressure, is expected to dominate at temperatures appropriate at 400 km ($1450^\circ \pm 150^\circ$ [*Verhoogen*, 1980]). Thus the effects of pressure may well reduce conductivity below the estimates shown in Figure 8.

Consequently, it seems necessary to invoke changes either in the conduction mechanism or the activation energy for the olivine/spinel system, at least deeper than ≈400 km. The induction data cannot distinguish between a transition over a wide depth range and a sharp (1 to 2 orders of magnitude) increase at the olivine-spinel phase transition. *Akimoto and Fujisawa* [1965] have demonstrated such a conductivity jump for this phase transition in faylite, and *Mao and Bell* [1977] show large differences in conductivity for the two phases of faylite at identical pressures. However, since iron content affects conduction in olivine so strongly [*Mao and Bell*, 1972, 1977], these results are of questionable relevance to the magnesium rich upper mantle. Once again it is clear that further laboratory studies are urgently needed.

5. CONCLUSIONS

In this paper we have used smooth, one-dimensional inversion routines to produce a range of mantle conductivity models, together with a linearized resolution analysis and constrained inversions to assess which model features are required by the Tucson MT data. We find that these data require an anomalously conductive zone (total conductance $\approx 10^4$ S) in the upper 200 km of the mantle. This may represent an aesthenospheric HCL, but the geometry of the conductive zone is not resolved. Conductivity is required to increase to ≈ 0.2–0.3 S m^{-1} between 200 and 600 km. The data allow, but do not require, this increase to occur as a step at the olivine-spinel phase transition at 400 km depth. An upper mantle which is resistive (0.05 S m^{-1} or less) between 200 and 700 km is ruled out. A further increase in conductivity to ≈ 1 S m^{-1} occurs between 600 and 900 km depth. Again, this increase could occur as a step at the 670 km seismic discontinuity, but models without this feature (including models with a sharp decrease at the same depth) are also acceptable. Below 1000 km, large-scale averages of log conductivity increase slowly. The average lower mantle conductivity between 700 and 1500 km is ≈ 1 S m^{-1}, within a factor of 2 or 3. In particular, a lower mantle which is very resistive throughout is not allowed by the data. Resolution length scales range from 200 to 500 km, with the best resolution (< 300 km) between 300 and 1000 km depth. These broad resolution lengths allow small-scale features with conductivities which deviate substantially from the large-scale average values given here.

Our analysis demonstrates that an extraordinary (and probably unattainable) increase in data quality would be required to truly resolve small scale features such as discontinuities in conductivity. However, localized (albeit large-scale) averages of conductivity are constrained much more tightly than a casual examination of the range of mantle conductivity models presented in the literature would suggest possible. With improved understanding of the connection between conductivity and other properties, these averages should be important clues to the composition and physical state of the Earth's mantle. Therefore we cannot overemphasize the need for more laboratory studies of electrical conductivity at high pressures and temperatures.

APPENDIX: LINEARIZED RESOLUTION ANALYSIS

The resolution kernels of Figure 4 are based on linearization of the one-dimensional MT inverse problem in the vicinity of the minimum roughness solution. As such, the standard interpretation of these kernels [e.g., *Backus and Gilbert*, 1970] is rigorously valid only for small perturbations to the smooth model. If the true Earth is very far from the smoothed model, the resolution kernels could potentially be misleading. *Smith and Booker* [1988] (hereafter SB) argue that for an appropriate choice of model parameters, this should not generally be a serious problem for minimum roughness MT inversions and that the resulting smooth conductivity models can reasonably be interpreted as the truth smoothed through the resolution kernels. Here we expand on this point and demonstrate its relevance to the Tucson MT data.

For simplicity we consider only models with a finite (but not necessarily small) number of layers p. We concentrate on the simpler case of finite precise data and only briefly indicate the effect of data errors. To set notation we first review resolution theory for linear inverse problems.

Linear Theory

Here the n-dimensional data vector $\mathbf{d}$ is related to the model $\mathbf{m}$ via the $n \times p$-dimensional matrix of data kernels $\mathbf{G}$:

$$\mathbf{d} = \mathbf{G}\mathbf{m} \tag{A1}$$

We seek a model $\mathbf{m}$ which minimize the roughness penalty

$$\|\mathbf{m}\|_{\mathbf{P}}^2 = \mathbf{m}^T\mathbf{P}\mathbf{m} \tag{A2}$$

subject to the data constraints of (A1). For the flattest and

smoothest models considered in this paper $\mathbf{P} = \mathbf{D}^T\mathbf{D}$ where $\mathbf{D}$ is a discrete approximation to the first or second derivative operator [cf. *Constable et al.*, 1987]. In general, we refer to this model as the P-smoothest model. Assuming for simplicity that $\mathbf{P}$ is invertible, the solution has the standard form [e.g., *Menke*, 1984]

$$\hat{\mathbf{m}} = \mathbf{P}^{-1}\mathbf{G}^T(\mathbf{G}\mathbf{P}^{-1}\mathbf{G}^T)^{-1}\mathbf{d} \tag{A3}$$

so that $\hat{\mathbf{m}}$ is related to the true model $\mathbf{m}$ via

$$\hat{\mathbf{m}} = [\mathbf{P}^{-1}\mathbf{G}^T(\mathbf{G}\mathbf{P}^{-1}\mathbf{G}^T)^{-1}\mathbf{G}]\mathbf{m} = \mathbf{R}\mathbf{m} \tag{A4}$$

where $\mathbf{R}$ is the $p \times p$ resolution matrix. The ith row of $\mathbf{R}$ is the resolution kernel $\mathbf{r}_i$ for the estimate of the ith model parameter $\hat{m}_i$, which is a weighted average, with weights r_{ij}, of the true model parameters m_j.

In the approach originally developed by *Backus and Gilbert* [1970], the resolution kernels play a fundamental role. They suggested optimizing resolution of the ith model parameter by finding resolution kernels $\mathbf{r}_i$ as linear combinations of the data kernels (i.e., the rows of $\mathbf{G}$) which are in some sense closest to a delta function. In our notation with a finite-dimensional model space we want

$$r_{ij} \approx \delta_{ij}$$

where δ_{ij} is the Kroenecker delta. In fact, it is readily shown that if the distance between the vectors $\boldsymbol{\delta}_i = (\delta_{i1}, \cdots, \delta_{ip})$ and $\mathbf{r}_i$ is defined as

$$(\mathbf{r}_i - \boldsymbol{\delta}_i)^T\mathbf{P}^{-1}(\mathbf{r}_i - \boldsymbol{\delta}_i)$$

the optimum resolution kernel is just the ith row of the matrix $\mathbf{R}$ defined in (A4).

When errors in the data are allowed, the hard constraints of (A2) are replaced by a condition that the data be fit adequately

$$\|\mathbf{d} - \mathbf{G}\mathbf{m}\| \le M^2 \tag{A2'}$$

and the resolution matrix becomes

$$\mathbf{R} = [\mathbf{P}^{-1}\mathbf{G}^T(\mathbf{G}\mathbf{P}^{-1}\mathbf{G}^T + \lambda\mathbf{I})^{-1}\mathbf{G}] \tag{A4'}$$

where λ is chosen so that equality in (A2') is achieved for the chosen tolerance M^2.

Linearized Resolution Matrix

For nonlinear problems, (A1) is replaced by

$$\mathbf{d} = \mathbf{L}(\mathbf{m}) \tag{A5}$$

where $\mathbf{L}$ represents an n-vector of data functionals, with Jacobian $\mathbf{J}$

$$J_{ij} = \frac{\partial L_i}{\partial m_j}.$$

For small perturbations $\delta\mathbf{m}$ from a model $\mathbf{m}_0$ the perturbation to the data satisfies

$$\delta\mathbf{d} = \mathbf{L}(\mathbf{m}_0 + \delta\mathbf{m}) - \mathbf{L}(\mathbf{m}_0) \approx \mathbf{J}\Big|_{\mathbf{m}_0}\delta\mathbf{m} \tag{A6}$$

Thus, to characterize resolution of small deviations from a known model $\mathbf{m}_0$, the linear theory can be used by replacing $\mathbf{G}$ by $\mathbf{J}$ in (A4) (or (A4')):

$$\mathbf{R} = [\mathbf{P}^{-1}\mathbf{J}^T(\mathbf{J}\mathbf{P}^{-1}\mathbf{J}^T)^{-1}\mathbf{J}] \tag{A7}$$

There is a more satisfying way to develop a linearized resolution analysis for P-smoothest models. For a fixed model $\mathbf{m}$, let $\mathbf{S}(\mathbf{m})$ be the model which minimizes (A2) subject to (A5). $\mathbf{S}$ is a generalized resolution operator. For linear problems, $\mathbf{S}$ reduces to the resolution matrix of (A4) and is independent of $\mathbf{m}$. More generally, $\mathbf{S}(\mathbf{m})$ is a projection operator in the sense that

$$\mathbf{S}[\mathbf{S}(\mathbf{m})] = \mathbf{S}(\mathbf{m}). \tag{A8}$$

We call the $p \times p$ Jacobian of $\mathbf{S}$ evaluated at $\mathbf{S}(\mathbf{m})$ the linearized resolution operator for $\mathbf{m}$

$$\mathbf{R}(\mathbf{m}) = \frac{\partial \mathbf{S}}{\partial \mathbf{m}}\Big|_{\mathbf{S}(\mathbf{m})} \tag{A9}$$

Note that $\mathbf{S}$ and $\mathbf{R}$ depend on $\mathbf{m}$ only through the data vector $\mathbf{d}$. In general, there will thus be a $p-n$ dimensional manifold of models mapped to a fixed P-smoothest model and corresponding linearized resolution matrix. By using the chain rule in (A8), it is readily verified that $\mathbf{R}(\mathbf{m})$ is a linear projection matrix ($\mathbf{R}\mathbf{R} = \mathbf{R}$). In fact, using the linearization of (A6) it can be verified that $\mathbf{R}(\mathbf{m})$ is given by the projection matrix of (A7) with the Jacobian $\mathbf{J}$ evaluated at $\mathbf{S}(\mathbf{m})$.

If $\mathbf{m}_0$ ($= \mathbf{S}(\mathbf{m}_0)$) is a smoothest model, it lies in the subspace spanned by the rows of the Jacobian evaluated at $\mathbf{m}_0$ [cf. *Constable et al.*, 1987; SB]. Since $\mathbf{R}(\mathbf{m}_0)$ projects onto this space, we have

$$\mathbf{R}(\mathbf{m}_0)\mathbf{m}_0 = \mathbf{m}_0 = \mathbf{S}(\mathbf{m}_0) \tag{A10}$$

i.e., smoothest models smoothed through the linearized resolution kernels reproduce themselves. (This is exactly true for the case of error free data considered here and approximately true when data errors are allowed.) SB conjecture that if the one-dimensional MT inverse problem is parametrized so that $\mathbf{m}$ gives the layer conductivities (as opposed to log conductivities), then (A10) can be approximately generalized to any conductivity model $\mathbf{m}$

$$\mathbf{R}(\mathbf{m})\mathbf{m} \approx \mathbf{S}(\mathbf{m}) \tag{A11}$$

Put differently, all models which result in the same data (including the unknown true model) when smoothed through the resolution kernels of the corresponding P-smoothest model approximately reproduce this smooth model. If this is true, the linearized resolution operator can be interpreted exactly as in the purely linear case, although the resolution depends, through the data, on the true model. We note that including the presence of errors complicates this qualitative discussion only slightly but may make the formal theory much more complicated. (For example, in this case the P-smoothest model depends on data errors as well as $\mathbf{m}$). Both the precise statement (e.g., in what sense should (A11) hold approximately?) and proof of this conjecture elude us. However, there are heuristic arguments which suggest that this conjecture should be valid in some way (see SB), and it is straightforward to empirically test (A11) by using the resolution kernels to smooth a range of models which are consistent with the data (see also examples of SB).

In Figure A1 we plot $\mathbf{R}(\mathbf{m}_0)\mathbf{m}_i$ for four models which approximately fit the Tucson data: $\mathbf{m}_0$ is the preferred (smoothest) model 4 from Figure 1; $\mathbf{m}_1$ is the (D^+) model which best fits all of the data (with error bars enlarged as for $\mathbf{m}_0$ as discussed in section 2. Note that this model, which consists of a series of spikes of finite conductance separated by perfectly resistive layers, is quite different from $\mathbf{m}_0$); $\mathbf{m}_2$ and $\mathbf{m}_3$ are models 3b and 3c. The shaded band gives the uncertainty in the model parameters arising from propagating the (adjusted) data errors into the smooth model. If the problem were completely linear, then for any model $\mathbf{m}$ which fits the data adequately we would expect $\mathbf{R}\mathbf{m}$ to lie at least approximately within these error bands. In fact, this condition is

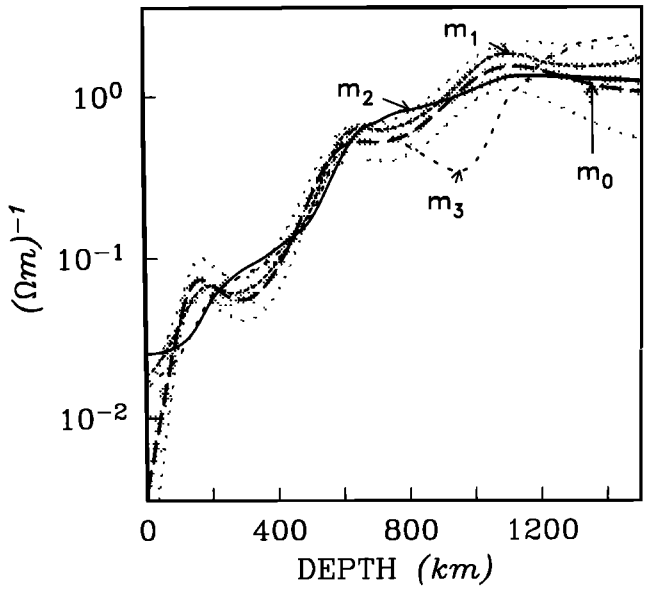

Fig. A1. Four mantle conductivity models $\mathbf{m}_i$, that approximately fit the Tucson data, averaged through the linearized resolution kernels, $\mathbf{R}(\mathbf{m}_0)$: $\mathbf{m}_0$, preferred smooth model 2d; $\mathbf{m}_1$, best fitting (D^+) model; $\mathbf{m}_2$, model (3b) with discontinuities; $\mathbf{m}_3$, model (3c) (with low-conductivity zone at the top of the upper mantle). The shaded region represents the two standard error swath for the smooth conductivity estimates. Note that these are estimates of the random errors in the conductivity averaged through the resolution kernels. Only these large-scale averages may be constrained by the data. With the exception of $\mathbf{m}_3$ near 1000 km (see discussion in text), all of the models have similar large scale average conductivities. This offers further empirical evidence that smooth models can be interpreted at least approximately as the true conductivity smoothed through the resolution kernels.

very nearly satisfied for all four models (including the unphysical D^+ model) with the linearized resolution operator. Significant deviations occur only for $\mathbf{m}_3$ at around 800-1000 km depth and for all models except $\mathbf{m}_0$ near the surface. However, the data predicted by $\mathbf{m}_3$ deviate significantly and systematically from the data for $3 < T < 20$ days (see Figure 3). Similarly, there is a great deal of scatter (greater than the data errors) in model responses at the shortest periods (Figure 3). It is thus likely that the deviations of the smoothed models from the error bounds can be ascribed to systematic deviations of the models in the data space rather than to serious violations of (A11). Although we have effectively enlarged the data errors to allow a fit within the expected χ^2 (see section 2), the error bars on the smooth model in Figure A1 are probably still too small. The failure of the one-dimensional model forces us to consider as acceptable a variety of models which differ systematically from each other in the data space. These systematic errors have a positive correlation for nearby frequencies, which should increase the size of the true error bars for the predicted model parameters. Note that similar problems would occur in a purely linear problem. Overall, these results suggest that (A11) does indeed hold approximately for models which fit the Tucson data.

As discussed by SB, (A11) will be reasonable only when the model parameters are the layer conductivities σ_i. When the model is parametrized in terms of $\log \sigma_i$, (A11) can fail severely. However, for models that vary by orders of magnitude, penalty functionals based on the roughness of $\log \sigma$ are preferable because they more effectively prevent the leakage of spurious structure from regions of high conductivity to regions of low-conductivity. SB thus suggested parametrizing the model in terms of σ (so that the linearized resolution analysis is valid) but changing the quadratic form that defines the roughness penalty from $\mathbf{P} = \mathbf{D}^T\mathbf{D}$ to $\mathbf{P}_w = \mathbf{D}^T\boldsymbol{\Sigma}^{-2}\mathbf{D}^T$ where $\boldsymbol{\Sigma} = \mathbf{diag}(\sigma_1, \cdots, \sigma_p)$. SB show that $\mathbf{P}_w$-smoothest σ models are essentially equivalent to P-smoothest $\log \sigma$ models. The linearized resolution kernels used to smooth the models in Figure A1 were derived using this weighted form of the roughness penalty.

The "deltaness criterion" implied by $\mathbf{P}_w$ corresponds to weighting deviations of the resolution kernels $\mathbf{r}_i$ from $\boldsymbol{\delta}_i$ in proportion to the model conductivity (see A7), so that for the $\mathbf{P}_w$-smoothest models, $\mathbf{r}_i$ is optimized to prevent leakage from regions of high conductivity. For these models, resolution kernels centered in a region of high conductivity may have large sidebands in regions of relatively lower conductivity. This is illustrated in Figure A2, where the kernel of the linearized resolution operator for the $\mathbf{P}_w$-smoothest σ model exhibits large sidebands below the diagonal. This pattern occurs because conductivity increases by several orders of magnitude with depth, so that large sidebands are allowed (by the $\mathbf{P}_w$-deltaness criterion) above the nominal depth of resolution.

Finally, we turn to the interpretation of resolution kernels computed for $\log \sigma$ P-smoothest models. Let $\mathbf{m} = \log \boldsymbol{\sigma}$, where the log is understood to act on each element of the vector of layer conductivities $\boldsymbol{\sigma}$, and let $\mathbf{S}_l(\mathbf{m})$ and $\mathbf{S}_w(\boldsymbol{\sigma})$, respectively, denote the P-smoothest $\log \sigma$ and $\mathbf{P}_w$-smoothest σ models that fit the data produced by conductivity profile $\boldsymbol{\sigma}$. Then with this notation the statement that the two approaches yield identical smooth models is

$$\mathbf{S}_l(\mathbf{m}) = \log \mathbf{S}_w(\boldsymbol{\sigma}) = \log \mathbf{S}_w(\exp \mathbf{m})$$

Applying the chain rule to evaluate the linearized resolution operators defined in (A9) yields

$$\mathbf{R}_l(\mathbf{m}) = \boldsymbol{\Sigma}^{-1}\mathbf{R}_w(\boldsymbol{\sigma})\boldsymbol{\Sigma} \qquad \text{(A12)}$$

where $\boldsymbol{\Sigma} = \mathbf{diag}(\mathbf{S}_w(\sigma)_1, \cdots, \mathbf{S}_w(\sigma)_p)$. In terms of the resolution matrix elements, (A12) is

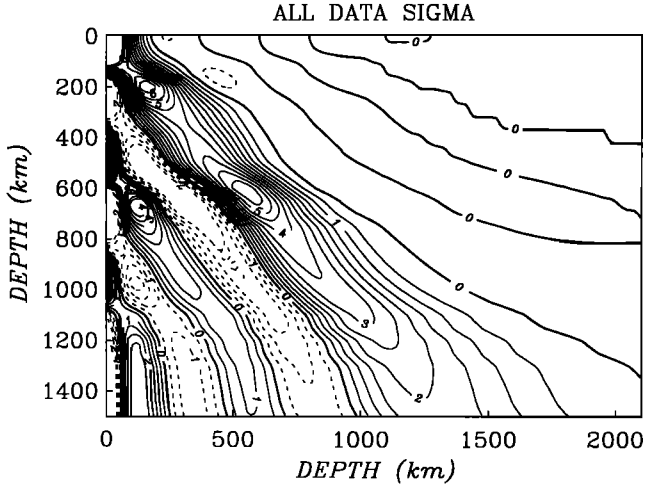

Fig. A2. Resolution kernels for the $\mathbf{P}_w$-smoothest conductivity model used for computing the large-scale averages plotted in Figure A1. The model is essentially identical to the P-smoothest log conductivity model ($\mathbf{m}_0$ in Figure A1). Because the resolution kernels for this model are chosen to limit leakage from regions of high conductivity, there are large sidebands in regions of relatively low conductivity above the nominal sampling depth (i.e., below the diagonal in the figure). The resolution kernels for the equivalent P-smoothest log conductivity model (Figure 4*b*) are proportional to these resolution kernels weighted by the smooth conductivity (see text).

$$r_{ij} = \frac{r_{wij}S(\sigma)_j}{S(\sigma_i)} = \frac{r_{wij}S(\sigma)_j}{\sum_j r_{wij}S(\sigma)_j} \quad \text{(A13)}$$

where the last step follows from (A10). Hence, assuming that (A11) holds approximately for the P_w-smoothest σ model, the jth element of the ith row of $\mathbf{R}_I$ gives an estimate of the fraction of conductance in the ith layer of the P-smoothest log σ model which comes from layer j.

Acknowledgments. J. C. Larsen provided much of the inspiration for the analysis reported here, as well as a copy of the Tucson electric field data. A. Schultz and T. Zhang assisted in the early phase of this work. S. C. Constable and J. T. Smith provided inversion routines. Support was provided by the National Science Foundation through grant EAR-8708401.

REFERENCES

Achache, J., J.L. Le Mouel, and V. Courtillot, Long period geomagnetic variations and mantle conductivity: an inversion using Bailey's method, *Geophys. J. R. Astron. Soc., 65*, 579-601, 1981.

Akimoto, S., and H. Fujisawa, Demonstration of the electrical conductivity jump produced by the olivine-spinel transition. *J. Geophys. Res., 70*, 443-449, 1965.

Anderson, D.L., Composition of the Earth, *Science, 243*, 367-370, 1989.

Backus, G., and J.F. Gilbert, The resolving power of gross Earth data, *Geophys. J. R. Astron. Soc., 16*, 169-205, 1970.

Banks, R.J., Geomagnetic variations and the electrical conductivity of the upper mantle, *Geophys. J. R. Astron. Soc., 17*, 457-487, 1969.

Constable, S.C., R.L. Parker, and C.G. Constable, Occam's inversion: a practical algorithm for generating smooth models from EM sounding data, *Geophysics, 92*, 633-648, 1987.

Dmitriev, V.I., and M.N. Berdichevsky, The fundamental model of magnetotelluric sounding, *Proc. IEEE, 67*, 1033-1044, 1979.

Duba, A.G., and T.J. Shankland, Free carbon and electrical conductivity in the Earth's mantle, *Geophys. Res. Lett., 9*, 1271-1274, 1982.

Egbert, G.D., J.R. Booker, and A. Schultz, Very long period magnetotellurics at Tucson observatory: Estimation of impedances, *J. Geophys. Res.*, this issue.

Ferguson, I.J., F.E.M. Lilley, and J.H. Filloux, Geomagnetic induction in the Tasman Sea and electrical conductivity structure beneath the Tasman seafloor, *Geophys. J. Int., 102*, 299-312, 1990.

Filloux, J.H., Ocean-floor magnetotelluric sounding over the North Central Pacific, *Nature, 269*, 297-301, 1977.

Filloux, J.H., North Pacific magnetotelluric experiments, *J. Geomagn. Geoelectr., 32 SI*, 33-44, 1980.

Gough, D.I., Mantle upflow under North America and plate tectonics, *Nature, 311*, 428-432, 1984.

Hobbs, B.A., Inversion of broad frequency band geomagnetic response data, *J. Geomagn. Geoelectr., 35*, 723-732, 1983.

Jady, R.J. and Paterson, G.A., Inversion methods applied to *Dst* data, *J. Geomagn. Geoelectr., 35*, 733-746, 1983.

Jones, A.G., Observations of the electrical aesthenosphere beneath Scandinavia, *Tectonophysics, 90*, 37-55, 1982.

Karato, S., The role of hydrogen in the electrical conductivity of the upper mantle, *Nature, 347*, 272-273, 1990.

Lahiri, B.N., and A.T. Price, Electromagnetic induction in nonuniform conductors, and the determination of the conductivity of the Earth from terrestrial magnetic variations, *Philos. Trans. R. Soc. London, Ser. A, 237*, 509-540, 1939.

Larsen, J.C., Low frequency (0.1-6.0 cpd) electromagnetic study of deep mantle conductivity beneath the Hawaiian Islands. *Geophys. J. R. Astron. Soc., 43*, 17-46, 1975.

Larsen, J.C., Removal of local surface conductivity effects from low frequency mantle response curves, *Acta Geodaet. Geophys. et Montanist. Acad. Hung., 12*, 183-186, 1977.

Larsen, J.C., Electromagnetic response functions from interrupted and noisy data, *J. Geomagn. Geoelectr., 32 SI*, 89-103, 1980.

Larsen, J.C., Transfer functions: smooth robust estimates by least squares and remote reference methods, *Geophys. J. Int., 99*, 655-663, 1989.

Li, X., and R. Jeanloz, Electrical conductivity of $(Mg,Fe)SiO_3$ perovskite and a perovskite-dominated assemblage at lower mantle conditions, *Geophys. Res. Lett., 14*, 1075-1078, 1987.

Li, X., and R. Jeanloz, Laboratory studies of the electrical conductivity of silicate perovskites at high pressures and temperatures, *J. Geophys. Res., 95*, 5067-5079, 1990*a*.

Li, X., and R. Jeanloz, High pressure-temperature electrical conductivity of magnesiowustite as a function of iron oxide concentration, *J. Geophys. Res., 95*, 21,609-21,612, 1990*b*.

Li, X., and R. Jeanloz, Phase identification and electrical conductivity of an H_2O-bearing silicate assemblage at lower mantle conditions, *Nature, 350*, 332-333, 1991*a*.

Li, X., and R. Jeanloz, Effect of iron content on the electrical conductivity of perovskite and magnesiowustite assemblages at lower mantle conditions, *J. Geophys. Res., 96*, 6113-6120, 1991*b*.

Mao, H.K., and P.M. Bell, Electrical conduction and the red shift of absorption in olivine and spinel at high pressure, *Science, 176*, 403-406, 1972.

Mao, H.K., and P.M. Bell, Techniques of electrical conductivity measurement to 300 kbar, in *High Pressure Research: Applications in Geophysics*, edited by M.H. Manghnani and S. Akimoto, 642 pp.., Academic, San Diego, Calif., 1977.

Menke, W., *Geophysical Data Analysis: Discrete Inverse Theory*, 260 pp., Academic, San Diego Calif., 1984.

Oldenburg, D.W., Conductivity structure of the oceanic upper mantle beneath the Pacific plate, *Geophys. Jour. R. Astron. Soc., 65*, 359-394, 1981.

Osipova, I.L., S.E. Hjelt, and L.L. Vanyan, Source field problems in northern parts of the Baltic Shield, *Phys. Earth Planet. Inter., 53*, 337-342, 1989.

Parker, R.L., The inverse problem of electrical conductivity in the mantle, *Geophys. J. R. Astron. Soc., 22*, 121-138, 1970.

Parker, R.L., The inverse problem of geomagnetic induction: Existence and construction of solutions based upon incomplete data, *J. Geophys. Res., 85*, 4421-4428, 1980.

Peyronneau, J., and J.P. Poirier, Electrical conductivity of the Earth's lower mantle, *Nature, 342*, 537-539, 1989.

Porath, H., and D.I. Gough, Mantle conductivity structures in the Western United States from magnetometer array studies, *Geophys. J. R. Astron. Soc., 22*, 261-275, 1971.

Roberts, R.G., The deep electrical structure of the Earth, *Geophys. J. R. Astron. Soc., 85*, 583-600, 1986.

Rokityansky, I.I., *Geoelectromagnetic Investigation of the Earth's Crust and Mantle*, 381 pp., Springer-Verlag, New York, 1982.

Schmucker, U., Anomalies of geomagnetic variations in the southwestern United States, *Bull. Scripps Inst. Oceanogr.*, 13, 1970.

Schock, R.N., A.G. Duba, and T.J. Shankland, Electrical conduction in olivine, *J. Geophys. Res., 94*, 5829-5839, 1989.

Schultz, A., and J.C. Larsen, Analysis of zonal field morphology and data quality for a global set of magnetic observatory daily mean values, *J. Geomagn. Geoelectr., 35*, 835-846, 1983.

Schultz, A., and J.C. Larsen, On the electrical conductivity of the Earth's interior I: mid-mantle response function computation, *Geophys. J. R. Astron. Soc., 88*, 733-761, 1987.

Schultz, A., and J.C. Larsen, On the electrical conductivity of the Earth's interior II: delineation of heterogeneity by application of extremal inverse solutions, *Geophys. J. Int., 102*, 565-580, 1990.

Shankland, T.J., R.J. O'Connel, and H.S. Waff, Geophysical constraints on partial melt in the upper mantle, *Rev. Geophys. Space Phys., 19*, 394-406, 1981.

Shankland, T.J., and A.G. Duba, Standard electrical conductivity of isotropic, homogeneous olivine in the temperature range 1200–1500°C, *Geophys. J. Int., 103*, 25-32, 1990.

Sherman, D.M., The high-pressure electronic structure of magnesiowustite (Mg, Fe)O: Applications to the physics and chemistry of the lower mantle, *J. Geophys. Res., 96*, 14,299-14,312, 1991.

Smith, J.T., and J.R. Booker, MT inversion for minimum structure, *Geophysics 53*, 1565-1576, 1988.

Tozer, D.C., The mechanical and electrical properties of Earth's aesthenosphere, *Phys. Earth Planet. Inter., 25*, 280-296, 1981.

Waff, H.S., Theoretical considerations of electrical conductivity in a partially molten mantle and implications for geothermometry, *J. Geophys. Res., 79*, 4003-4010, 1974.

Waff, H.S., Effects of the gravitational field on liquid distribution in partial melts within the upper mantle, *J. Geophys. Res., 85*, 1815-1825, 1980.

Wannamaker, P.E., J.R. Booker, A.G. Jones, A.D. Chave, J.H. Filloux, H.S. Waff, and L.K. Law, Resistivity cross section through the Juan de Fuca subduction system and its tectonic implications, *J. Geophys. Res., 94*, 14,127-14,145, 1989.

Verhoogen, J., *Energetics of the Earth*, 139 pp., National Academy of Sciences, Washington D.C., 1980.

Weidelt, The inverse problem of geomagnetic induction, *Z. Geophys., 38,* 257-289, 1972.

Wilson, J.T., On the building and classification of mountains, *J. Geophys. Res., 95*, 6611-6628, 1990.

Wood, B.J., and J. Nell, High-temperature electrical conductivity of the lower-mantle phase (Mg, Fe)O, *Nature, 351*, 309-311, 1991.

J.R. Booker, Geophysics Program AK-50, University of Washington, Seattle WA 98195.

G.D. Egbert, College of Oceanography, Oregon State University, Oceanography Admin. Bldg. 104, Corvallis, OR, 97330-5503.

(Received July 9, 1991;
revised March 1, 1992;
accepted May 2, 1992.)